TECHNISCHE MECHANIK, Band 22, Heft 2, (2002), 79-88
Manuskripteingang: 18. Januar 2002

Elastic and Plastic Behavior of Model Solids

S. Hess, M. Kröger

A short ranged attractive (SHRAT) potential is employed here which is of the type of the effective two-particle interaction used in a variant of the 'embedded atom' method for metals. Properties of the (pure) SHRAT model system in its gaseous, (metastable) liquid, and solid states have been computed earlier by molecular dynamics and, where possible, successfully compared with analytical calculations, as well as with the behavior of real substances. After some remarks on scaling and reference values, elastic properties of the model metal are characterized by the bulk and shear moduli, and their corresponding Born-Green and fluctuation contributions. It is demonstrated that plastic flow implies significant structural changes, being reflected by the Born–Green contribution to the cubic shear modulus. Not only stick-slip behavior, but the detailed elastic response and plastic flow of the model solid is analyzed. In order to interpret and reproduce the simulated rheological quantities, a simple, but generalized Maxwell model is tested. Its tensorial generalization may be used in simulation schemes such as smoothed particle dynamics, which are applicable on length and time scales significantly larger than those accessible in molecular dynamics simulations.

1 Introduction

It is desirable to explain the thermo-physical properties of matter and the dynamic phenomena occurring in non-equilibrium processes on the basis of the properties of atoms and molecules and their interactions. During the last decades, the standard methods of thermodynamics (e.g. Muschik (Ed.) 1993) and statistical physics have been complemented by molecular dynamics (MD) and Monte Carlo (MC) computer simulations (Binder et al., 1996). Here the elastic behavior under shear and the transition to plastic flow in the solid are studied for a simple but representative model system.

2 The Interaction Potential

2.1 General Remarks and Special Model

Systems composed of (effectively) spherical particles have been modelled with potentials which are linear combinations of inverse powers of the distance r between two particles. Both the repulsion at short distances and the attraction at larger distances are described in this way. The distance where the potential vanishes defines a characteristic length, the diameter r_0 of a particle. Such potentials have already been used almost a century ago by G. Mie and E. Grüneisen and about two decades later by J.E. Lennard–Jones. They are commonly referred to as Lennard-Jones (LJ) potentials. In computer simulations, these potentials are usually cut off at a finite distance h, e.g. at $h = 2.5\,r_0$. Shorter cut-off distances are preferred in non-equilibrium molecular dynamics (NEMD) simulations. The potential has to be shifted such that it vanishes at $r = h$ and, for MD simulations, it is desirable that also the force vanishes at the cut-off distance. Here we use an alternative functional form for the potential with an even smoother cut-off (Hess, 1996; Hess and Kröger, 2000), viz. the short range attractive polynomial potential function SHRAT. It has a repulsive and a relatively short range attractive part ($h = 1.5\,r_0$). Properties of the model system in its gaseous, (metastable) liquid, and solid states were recently computed by MD and NEMD simulations and, where possible, compared with analytical calculations, as well as the behavior of real substances (Hess and Kröger, 2001).

For comparison the standard $6-12$ Lennard-Jones (LJ) potential is stated:

$$\phi^{\mathrm{LJ}}(r) = 4\,\Phi_0\,((r/r_0)^{-12} - (r/r_0)^{-6})\,. \tag{1}$$

The quantities Φ_0 and r_0 set the characteristic energy and length scales. The SHRAT potential reads

$$\phi^{\mathrm{SHRAT}}(r) \sim 3\,(h-r)^4 - 4\,(h-r_{\min})\,(h-r)^3\,, \tag{2}$$

	e_b [eV]	r_0 [nm]	mass [10^{-27} kg]	$T_{\rm ref}$ [K]	$n_{\rm ref}$ [nm^{-3}]	$p_{\rm ref}$ [10^6 Pa]	$v_{\rm ref}$ [m/s]	$t_{\rm ref}$ [10^{-12} s]	$\dot\gamma_{\rm ref}$ [10^9 s^{-1}]
Ar	0.08	0.34	66.7	160	25.4	40.7	182	18.7	53.5
SM	3.5	0.23	106	6800	82.2	5590	940	2.45	410

Table 1: The characteristic reference values needed to convert the dimensionless variables used in the calculations to physical quantities (for an 'Argon-like' and a 'Standard' material).

for $r \le h$ and $\phi^{\rm SHRAT}(r) = 0$ for $r > h$. This function has a minimum at $r = r_{\rm min}$. Its intersection with the horizontal axis is $r_0 = (4/3)r_{\rm min} - (1/3)h$. This functional form has been used for the effective two-particle interaction in a variant of the 'embedded atom' method for metals (Hoover and Hess, 1999; Kröger and Hess, 2000). If one requires, as in (Hess, 1996), that the force at $r = r_0$ and the depth of the potential at $r = r_{\rm min}$ be equal to the corresponding LJ-values, one finds $h = (113/81)r_0 \approx 1.4\,r_0$, $r_{\rm min} = (89/81)r_0 \approx 1.1\,r_0$. The resulting potential is $24\,\Phi_0(1 - r/r_0)((h-r)/(h-r_{\rm min}))^3$. Here we choose the similar values $h = (3/2)r_0$, $r_{\rm min} = (9/8)r_0$ and set the depth of the potential equal to Φ_0, in analogy to the LJ-potential. Then we have

$$\phi^{\rm SHRAT}(r) = (512/27)\,\Phi_0\,(1 - r/r_0)\,(3 - 2\,r/r_0)^3, \;\; r \le 1.5\,r_0\,, \tag{3}$$

and $\phi^{\rm SHRAT}(r) = 0$ for $r > 1.5\,r_0$. In units of Φ_0/r_0, the force at $r = r_0$ is $512/27 \approx 19$. The corresponding value for the LJ=potential is 24. Notice that this potential is finite at $r = 0$, viz. $\phi^{\rm SHRAT}(0) = 512\,\Phi_0$. For temperatures less than $10\,\Phi_0/k_{\rm B}$, this is of no practical concern since the Boltzmann factor $\exp(-\Phi_0/k_{\rm B}T)$ governing the fraction of particles which can reach this distance is smaller than 6×10^{-23}. In numerical calculations and in the graphs to be displayed here, all physical quantities are expressed in the standard LJ units used by Hoover (1986,1993), Allen and Tildesley (1987), Evans and Morris (1990), Haberlandt et al. (1995), e.g., lengths and energies are given in units of r_0 and Φ_0. The dimensionless variables are denoted by the same symbols as the corresponding physical quantities when there is no danger of confusion.

In dimensionless notation, the LJ and SHRAT potentials read

$$\phi^{\rm LJ}(r) = 4\,(r^{-12} - r^{-6})\,, \tag{4}$$

and

$$\phi^{\rm SHRAT}(r) = (512/27)\,(1 - r)\,(3 - 2\,r)^3, \;\; r \le 3/2, \tag{5}$$

whereas $\phi^{\rm SHRAT}(r) = 0$ for $r > 3/2$. Similarly, the number density $n = N/V$, where N and V are the number of particles and the volume of the system, and the temperature T are expressed in units of $n_{\rm ref} = r_0^{-3}$ and $T_{\rm ref} = \Phi_0/k_{\rm B}$, respectively. The unit for the pressure is $p_{\rm ref} = \Phi_0\,r_0^{-3}$.

2.2 Scaling and Reference Values

If one wants to compare properties as computed here with those of real materials, one has to specify the parameters of the interaction potential, viz. the well depth Φ_0, the characteristic length r_0 and the mass m of the particles. It is not our intention to mimic a particular substance but to provide a feeling for the order of magnitude of the reference quantities for various cases of interest. As an estimate for Φ_0 and r_0, one can use one sixth of the binding energy e_b of an atom and the inverse of the cubic root of the number density, respectively, of the low temperature solid. Two sets of values are presented in Table 1. The first one is the familiar Argon-like substance, referred to as Ar. The second one, referred to as SM (for Standard Material), is copper-like since the values for the characteristic energy, distance, and mass are chosen to match those of copper. As far as the order of magnitudes are concerned, these values are typical for many solid materials one can touch everyday. The coinage metals like silver, copper, gold, iron, and nickel have rather similar binding energies and interparticle distances, viz. $3.0, 3.5, 3.8, 4.3, 4.4$ eV and $0.26, 0.23, 0.26, 0.23, 0.22$ nm. Of course, a true modelling of these materials requires more complicated potential functions. As input are used in Table 1: either the binding energy e_b or the temperature $T_{\rm ref} = \Phi_0/k_{\rm B} = e_b/(6\,k_{\rm B})$ associated with the potential well depth, either the diameter r_0 or the number density $n_{\rm ref} = r_0^{-3}$, and the mass m. The derived reference quantities which are listed here are $p_{\rm ref}$ for the pressure, the stress and for elasticity coefficients, $v_{\rm ref}$ and $t_{\rm ref}$ for the velocity and the time, as well as $\dot\gamma_{\rm ref}$ for the shear rate.

2.3 Remarks on MD Simulations

Here results are presented which are inferred from simulations at a constant temperatures and for a constant number density $n = N/V$ (NVT simulations) typical for a solid state. The calculations were performed for $N = 4 \cdot 8^3 = 2048$ particles, where the initial positions were face centered cubic (fcc) lattice sites. The equations of motion were integrated with the velocity Verlet algorithm with the time step $\delta t/t_{\rm ref} = 0.005$. The LJ reference time is $t_{\rm ref} = r_0\,(m/\Phi_0)^{(1/2)}$, and m is the mass of a particle. A cubic simulation box with volume V and periodic boundary conditions have been used. The temperature was kept constant by rescaling the magnitude of the particle velocities which corresponds to the Gaussian constraint of constant kinetic energy. Typically, the system was aged for 2000 or more time steps corresponding to 10 or more reduced time units, before the data for equilibrium properties were extracted as time averages over 4000 or more time steps corresponding to 20 or more time units.

The pressure $p = nk_{\rm B}T + p^{\rm pot}$ is the sum of the kinetic or ideal gas contribution $nk_{\rm B}T$ and the potential contribution $p^{\rm pot}$. The latter quantity is computed according to

$$V\,p^{\rm pot} = \frac{1}{3}\left\langle \sum_i \mathbf{r}^i \cdot \mathbf{F}^i \right\rangle = \frac{1}{3}\left\langle \sum_{i<j} \mathbf{r}^{ij} \cdot \mathbf{F}^{ij} \right\rangle . \tag{6}$$

The bracket indicates a time average. Here $\mathbf{F}^i = \sum_{j\neq i} \mathbf{F}^{ij}$ is the force acting on particle i, $\mathbf{F}^{ij} = \mathbf{F}(\mathbf{r}^{ij})$ is the force exerted on particle i from particle j, and $\mathbf{F}(\mathbf{r}) = -\partial\,\phi(\mathbf{r})/\partial\,\mathbf{r}$. The symbol $\sum_{i<j}$ means a double summation over pairs of particles, with i less than j.

3 Elasticity Coefficients

The elastic properties of an effectively isotropic solid are characterized by the (isothermal) bulk modulus or compression modulus $B = n\,(\partial p/\partial n)_T$ and by the shear modulus G. The Born–Green expression (Born, 1939, 1940; Green, 1952,1954) for the latter quantity, used in MD-simulations, is the time average of a two-particle quantity, viz.

$$G^{\rm BG} = \frac{1}{15\,V}\left\langle \sum_{i<j} \left(r^{-2}\left(r^4\phi'\right)'\right)^{ij} \right\rangle , \tag{7}$$

where the prime denotes the derivative with respect to r. This high frequency shear modulus is also non–zero in the fluid state (Zwanzig and Mountain, 1965). Sometimes it is referred to as Maxwell shear modulus. The low frequency shear modulus G, which is non–zero in the solid state but vanishes in the fluid state, is computed according to $G = G^{\rm BG} + G^{\rm fluct}$ (Squire et al., 1969; Hoover et al., 1969; Schoen et al., 1995). The (negative) fluctuation contribution $G^{\rm fluct}$, involves a time average of the square of a two-particle quantity, thus it contains three- and four-particle contributions.

In cubic systems, the anisotropy of the shear modulus implies that one needs two coefficients to characterize the shear behavior. These can e.g. be the largest and smallest values (for fcc and bcc) c_{44}, in Voigt notation, and $\tilde{c}_{44} = (c_{11} - c_{12})/2$. The modulus c_{44} is associated with a displacement and its gradient parallel to the (100) and (010)-directions. The shear modulus $\tilde{c}_{44}$ pertains to a deformation where the displacement and its gradient enclose an angle of 45 degrees with the (100) and (010)-directions. The expressions used for the computation of the Born–Green and fluctuation contributions of c_{44} are

$$V\,c_{44}^{\rm BG} = \left\langle \sum_{i<j} \left(\frac{1}{2}(x^2+y^2)\,r^{-1}\phi' \right)^{ij} \right\rangle + \left\langle \sum_{i<j} \left(x^2\,y^2\,r^{-1}\left(r^{-1}\phi'\right)' \right)^{ij} \right\rangle , \tag{8}$$

and

$$V\,c_{44}^{\rm flct} = -\frac{1}{k_{\rm B}T}\left[\left\langle \left(\sum_{i<j} \left(x\,y\,r^{-1}\phi'\right)^{ij} \right)^2 \right\rangle - \left(\left\langle \sum_{i<j} \left(x\,y\,r^{-1}\phi'\right)^{ij} \right\rangle \right)^2 \right] . \tag{9}$$

For $\tilde{c}_{44}$ one uses similar expressions with xy replaced by $(x^2 - y^2)/2$. A measure for the anisotropy of the shear modulus is the ratio $c_{\rm anis} = c_{44}/\tilde{c}_{44}$. For an effectively isotropic solid one has $c_{\rm anis} = 1$, many monocrystalline

B	c_{44}	G	G_c	$c_{44}^{\rm BG}$	$G^{\rm BG}$	$G_c^{\rm BG}$
44.8 ± 0.5	35.8 ± 0.3	28.6 ± 0.2	-18.2 ± 0.2	41.0 ± 0.1	32.9 ± 0.1	-20.2 ± 0.1

Table 2: The isothermal bulk modulus B and shear moduli, all in units of the reference pressure $p_{\rm ref}$, as computed in the MD simulation. The superscript BG refers to the Born–Green expression for the shear moduli.

cubic (fcc and bcc) substances exhibit values between 2 and 4, but both smaller and larger values also occur.

Alternatively, one describes the shear behavior of a cubic solid by the orientationally averaged shear modulus $G = (3c_{44} + 2\tilde{c}_{44})/5$ and the cubic modulus $G_c = \tilde{c}_{44} - c_{44}$. Its Born–Green contribution is given by

$$G_c^{\rm BG} = \frac{5}{12\,V} \left\langle \sum_{i<j} \Big(H(\mathbf{r})\, r^{-1} \left(r^{-1}\phi' \right)' \Big)^{ij} \right\rangle . \tag{10}$$

The quantity $H(\mathbf{r}) = x^4 + y^4 + z^4 - \frac{3}{5} r^4$ is a cubic harmonic. The bulk modulus of a cubic system is linked with the Voigt elasticity coefficients by $B = (c_{11} + 2\,c_{12})/3$. Just as the shear moduli, the isothermal bulk modulus is the sum of a Born–Green and a (negative) fluctuation contribution: $B = B^{\rm BG} + B^{\rm fluct}$ with $B^{\rm BG} = 5\,G^{\rm BG}/3 + 2\,p^{\rm pot}$, and

$$V\,B^{\rm flct} = -\frac{1}{9\,k_{\rm B}T} \left[\left\langle \left(\sum_{i<j} \left(r\phi' \right)^{ij} \right)^2 \right\rangle - \left(\left\langle \sum_{i<j} \left(r\phi' \right)^{ij} \right\rangle \right)^2 \right] . \tag{11}$$

Frequently the elastic behavior of an effectively isotropic solid is also characterized by Young's elasticity modulus E and Poisson's ratio ν. These quantities are linked with the bulk modulus and the orientationally averaged shear modulus G by $E = 9\,B\,G/(3\,B + G)$ and $\nu = (1/2)(3\,B - 2\,G)/(3\,B + G)$. In the fluid state one has $G = 0$ and consequently $E = 0$ and $\nu = 0.5$. For two-particle interactions, zero temperature and zero pressure the Cauchy relation $B = 5\,G/3$ applies. Then one has $E = 5\,G/2$ and $\nu = 0.25$. Solid Argon has the somewhat larger Poisson's ratio 0.30. At low temperatures, one has $\nu = 0.27$ for Fe and Ni, and $\nu = 0.22$ for Si. Rather large and small values are $\nu = 0.41$ for gold and $\nu = 0.07$ for diamond.

For low temperatures, the elasticity coefficients can be inferred from the change of the energy when the ideal lattice is subjected to the appropriate deformation. Alternatively, one may use the Born–Green expression involving the first and second derivatives of the potential to compute the coefficients in the undistorted state. Results of such calculations are presented by Hess and Kröger (2001). The values for elasticity coefficients as inferred from MD simulations for the solid at the temperature $T/T_{\rm ref} = 0.6$ and the density $n/n_{\rm ref} = 0.942$ are given in Table 1 in units of $p_{\rm ref}$. At this state, the average potential energy per particle $e^{\rm pot}$ and the pressure are $e^{\rm pot}/\Phi_0 = -4.950$, $p/p_{\rm ref} = 0.02$. The value of the shear modulus c_{44} as inferred from G and G_c according to $c_{44} = G - 2G_c/5$ agrees with the directly extracted value within the computational uncertainty. The same applies to the Born–Green contributions to these quantities. For the shear modulus $\tilde{c}_{44}$ one infers from $\tilde{c}_{44} = G + 3G_c/5$ the value 17.7 ± 0.3, in units of $p_{\rm ref}$. The resulting anisotropy coefficient is $c_{\rm anis} = c_{44}/\tilde{c}_{44} \approx 2.0$. The Young's modulus E and Poisson's ratio ν as computed from the values for B and G given in Table 2 are $E \approx 71$, in units of $p_{\rm ref}$, and $\nu \approx 0.24$. The ratio G/B is ≈ 0.64.

4 Elastic Behavior and Plastic Flow

4.1 Remarks on Non–equilibrium Molecular Dynamics Simulations

The method of Non–equilibrium molecular dynamics (NEMD) has been developed and applied to various problems during the last three decades, for books on this subject see Hoover (1986,1991), Allen and Tildesley (1987), Evans and Morris (1990), or Haberlandt et al. (1995). Methods which have previously been applied to fluids can be adapted to the study of solids. Here, we consider a simple shear deformation in the x-direction with a constant (average) shear rate. The (average) gradient of the velocity $\mathbf{v}$ is in the y-direction. The shear rate $\dot{\gamma}$ is given by $\dot{\gamma} = \partial v_x/\partial y$. Such a shear flow can be generated either by moving boundaries or by forces (see Ashurst and Hoover (1972, 1975), Hoover and Ashurst (1975), Gosling et al. (1973), Hess and Loose, 1989), or as applied

here, by moving image particles undergoing an ideal Couette flow with the prescribed shear rate (homogeneous shear). Let the deformation be switched on at $t = 0$. Then, at time t the image particles above (below) the basic (central) box have moved in the x-direction to the right (left) by the distance $\dot{\gamma}\, t\, L$ modulo(L), where L is the length of the periodicity box in the y-direction. Of course, the periodic boundary conditions for the particles leaving and entering the basic box have to be modified (Lees-Edwards boundary conditions, Lees and Edwards, 1972). For a system in a fluid state in equilibrium and for not too large shear rates, a linear velocity profile typical for a plane Couette flow is set up in the basic box (from which the data are extracted). At high shear rates in a fluid and for moderate shear rates in solids, also a plug-like flow occurs. Then it is essential to use a velocity profile unbiased thermostat (PUT), cf. Hoover (1983), Evans and Morris (1984), Evans and Hoover (1986), Loose and Hess (1989, 1990), Hess and Loose (1989, 1990). A shear flow can also be generated by modifying the equations of motion (SLLOD), cf. Hoover (1986, 1991), Allen and Tildesley (1987), Evans and Morris (1990), Haberlandt et al. (1995). For reviews of NEMD results for rheological properties of simple and of complex fluids see Hess et al. (1996, 1997) and Hess (2000).

Rheological properties such as the (non–Newtonian) viscosity and the normal pressure differences are obtained from the cartesian components of the stress tensor $\sigma_{\mu\nu} = -p_{\mu\nu}$ or of the pressure tensor $p_{\mu\nu}$ which is the sum of kinetic and potential contributions: $p_{\mu\nu} = p^{\rm kin}_{\mu\nu} + p^{\rm pot}_{\mu\nu}$,

$$V p^{\rm kin}_{\mu\nu} = \left\langle \sum_i m\, c^i_\mu c^i_\nu \right\rangle \ , \ \ V p^{\rm pot}_{\mu\nu} = \frac{1}{2} \left\langle \sum_{ij} r^{ij}_\mu F^{ij}_\nu \right\rangle . \tag{12}$$

Here $\mathbf{c}^i$ is the peculiar velocity of particle i, i.e. its velocity relative to the flow velocity $\mathbf{v}(\mathbf{r}^i)$, $\mathbf{r}^{ij} = \mathbf{r}^i - \mathbf{r}^j$ is the relative position vector of particles i, j and $\mathbf{F}^{ij}$ is the force acting between them. As before, the Greek subscripts μ, ν, which assume the values $1, 2, 3$, stand for cartesian components associated with the x, y, z-directions. In the simulations, the expression for the pressure tensor given is averaged over many (10^2 to 10^6) time steps. From the simulation, the kinetic and potential contributions to the pressure tensor and to the viscosity can be computed separately. Only the sum can be measured in a real experiment. The kinetic contribution to the viscosity dominates in dilute gases, cf. Loose and Hess (1988). In dense fluids (liquids) and solids the potential contribution is more important. Normal stress or pressure differences, e.g. $\sigma_{xx} - \sigma_{yy} = p_{yy} - p_{xx}$, have also been computed.

The visco–elastic behavior of a fluid is revealed by the growth of the shear stress in response to a shear deformation $\gamma = \dot{\gamma} t$, which is switched on at $t = 0$. Results for the liquid are presented by Hess and Kröger (2001). Here the attention is focused on the solid state.

4.2 Elastic Response and Plastic Flow of the Solid

The elastic response and the plastic yielding of a solid at the temperature $T/T_{\rm ref} = 0.6$ and the density $n/n_{\rm ref} = 0.942$, where the pressure is approximately zero, is presented next. More specifically, the shear stress is analyzed as function of the time for a linearly growing displacement with various shear rates. For small shear rates, the elastic behavior and the occurrence of the yield point are approximately independent of the shear rate. The plastic flow behavior beyond this point, however, does depend on $\dot{\gamma}$. This is shown in Fig. 1 where the shear stress is displayed as function of the time for the shear rates $\dot{\gamma}/\dot{\gamma}_{\rm ref} = 0.001$ and 0.005. The start is from an aged state which reached equilibrium. In all cases the end times are chosen such that one has a shear deformation $\gamma = 1.0$. The full and the dashed straight lines through the origin describe the elastic behavior with the full shear modulus c_{44} and the Born–Green contribution to this modulus. At the smaller shear rate one observes a pronounced stick–slip flow, at higher shear rates a more continuous plastic flow occurs. The effective viscosity inferred from the long–time average of the shear stress (or about one fifth of the maximum stress at the yield point) divided by the shear rate is about three orders of magnitude larger than the viscosities in the liquid state.

The stick–slip behavior, seen at the smaller shear rate, shows 8 maxima of the shear stress over a shear deformation $\gamma = 1$. The periodicity box contains 2×8 layers of particles, the displacement between opposite sides of the box is $\gamma_{\rm box} = 8\gamma$. Slips obviously occur when $\gamma_{\rm box}$ exceeds 1. Thus the eightfold repetition seems to be associated with the size of the system. The initial yielding at deformations just above 0.10, however, occurs for all shear rates shown. The latter phenomenon is an intrinsic property of the solid, and it seems reasonable in view of the Lindemann criterion which says that a crystal will melt when the displacement of atoms exceeds about one tenth of the lattice constant. Of course, it is desirable to study the plastic flow at longer times and to analyze the structural changes.

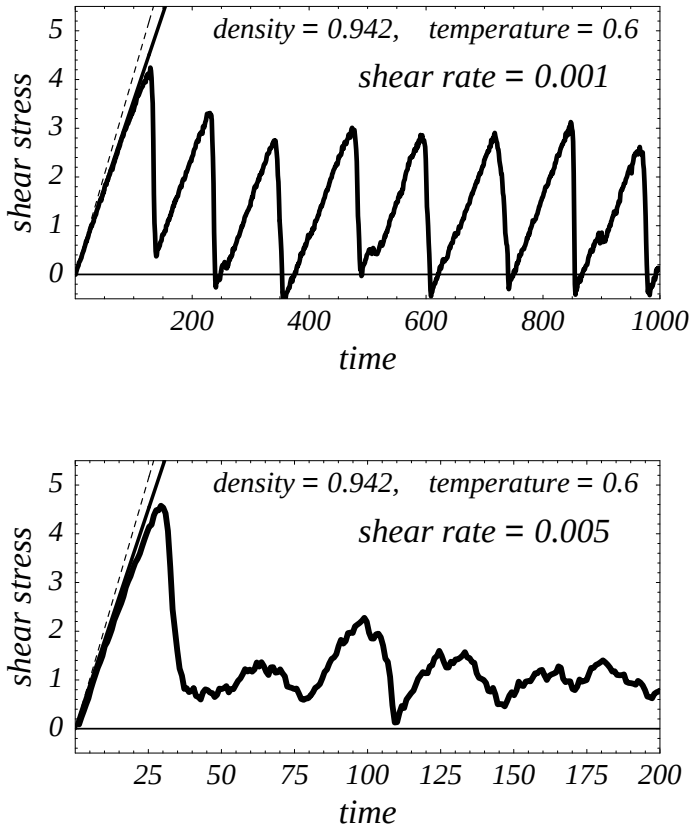

Figure 1: The shear stress, in the solid phase, as function of the time for the shear rates $\dot{\gamma} = 0.001, 0.005$. All physical quantities are in standard LJ–units.

In the upper graph of Fig. 2, the shear stress, for the shear rate $\dot{\gamma} = 0.005$, is displayed as function of the time up to 2000 time units corresponding to the shear deformation $\gamma = 10$. The plastic flow implies significant structural changes. This is reflected by the Born–Green contribution to the cubic shear modulus G_c, shown in the lower graph of Fig. 2. After about 250 time units, a significant structural change sets in. It leads to an increase of G_c which changes sign at about 500 time units, and then the system reaches a state where G_c is positive. The specific heat, inferred from the energy fluctuations, and the bulk modulus as displayed in Fig. 3 also signal this dramatic change which occurs at about 250 time units. Notice that a negative bulk modulus indicates a mechanically instable state.

Inspection of the positional order for times larger than about 500 time units reveals that the particles are rearranged such that practically densely packed (111)-layers are sliding over each other. The expression (10) for $G_c^{\rm BG}$ shows why this quantity is an ideal indicator for such structural changes. The main contribution to the average to be evaluated in (10) stems from particles in the first coordination shell, and an educated guess is

$$G_c^{\rm BG} \approx h\,\frac{5}{12V}\,\left\langle \sum_{i<j} \left(r^3 \left(r^{-1}\phi' \right)' \right)^{ij} \right\rangle = \frac{25}{4} h\,\left(p^{\rm pot} + G^{\rm BG} \right).$$

Here h is the (orientational) average of the quantity $H(\mathbf{r})\, r^{-4}$, taken over the particles in this shell. For an ideal fcc lattice with the axes parallel to the coordinate axes one has $h = -0.1$. For the previously mentioned layers normal to the gradient of the velocity, one finds $h = 0.012$ and $h = 0.029$ when one assumes that the layers above and below undergo zigzag or straight motions through the grooves as discussed by Ackerson and Loose (1994) and stay in the vicinity of the highest and lowest points on their path for equal time. When one takes into account that the motion is slowed down close to highest points and one weights the contributions from these positions with factors $2/3$ and $1/3$, one obtains $h = 0.033$ and $h = 0.044$, instead. The dashed and solid horizontal lines in the lower graph of Fig. 2 are based on these estimates for the values of h associated with the zigzag and the straight motions of layers of atoms. Structural changes can also be analyzed via the static structure factor (Hess et al., 1989) which

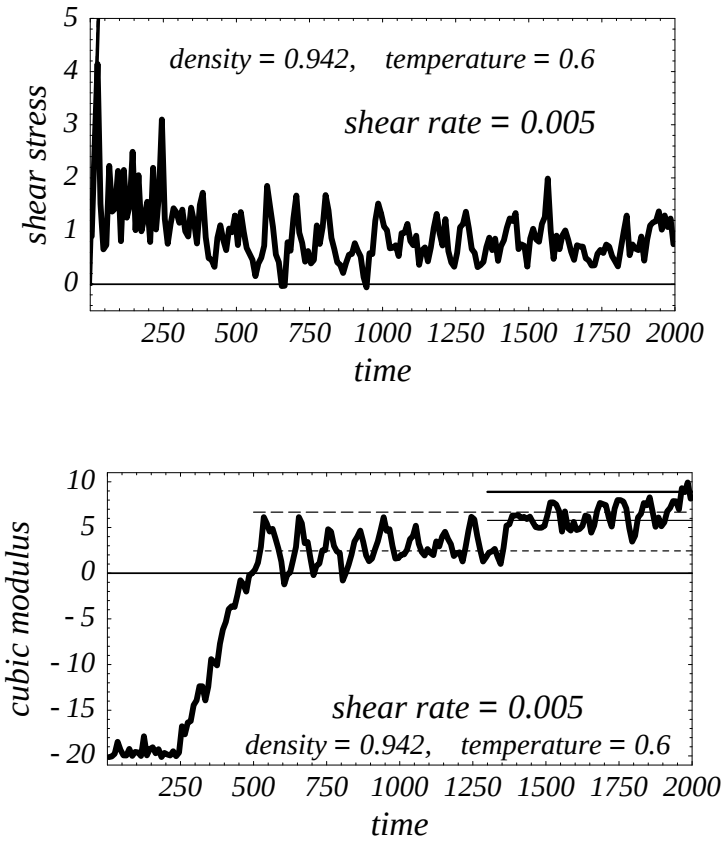

Figure 2: The shear stress and the cubic shear modulus G_c, in the solid phase, as function of the time for the shear rate $\dot{\gamma} = 0.005$. All physical quantities are in standard LJ–units.

is measured in scattering experiments. A more detailed structural analysis, as performed by Stankovic et al. (2001) for model metals is beyond the scope of the present article.

5 Modelling the Elastic–plastic Behavior

The transition from the elastic to the plastic behavior can be modelled by a generalized Maxwell- or Maxwell-Kelvin-Voigt model for the shear stress σ:

$$\tau_{\rm M}\,\partial\sigma/\partial t - \xi^2\,\Delta\,\sigma + \sigma = \eta(\dot{\gamma})\,\dot{\gamma} + G(\gamma)\,\gamma\,.$$

Here, the shear modulus $G(\gamma)$, the (effective) viscosity $\eta(\dot{\gamma})$, the Maxwell relaxation time $\tau_{\rm M}$ and the characteristic length ξ are model parameters. The low frequency shear modulus $G(\gamma)$ has to be chosen such that it vanishes for shear deformations γ larger than a characteristic value γ_c. A reasonable choice is $G(\gamma) = G_0\,(1 + 2(\gamma/\gamma_c)^\mu)\,(1 - (\gamma/\gamma_c)^\mu)^2$, for $\gamma \leq \gamma_c$, with a suitable exponent $\mu > 1$, and $G(\gamma) = 0$ for $\gamma > \gamma_c$. Here $G_0 = c_{44} = 36\,p_{\rm ref}$ is the relevant shear modulus of the linear elastic regime discussed above.

In Fig. 4 the shear stress computed in the NEMD simulation for $\dot{\gamma} = 0.0087$ is compared with curves calculated by this model with $\xi = 0$. The value for the viscosity is inferred from $\sigma_{\rm plast}/\gamma$ where $\sigma_{\rm plast} \approx 1.0\,p_{\rm ref}$ is the average shear stress in the plastic flow regime. The relaxation time is determined by $\tau_{\rm M} = \eta/c_{44}^{\rm BG}$ with $c_{44}^{\rm BG} = 41\,p_{\rm ref}$. The dashed and the solid curves pertain to $\mu = 2$, $\gamma_c = 0.19$ and $\mu = 4$, $\gamma_c = 0.23$, respectively. The solid curve provides a reasonable approximation. The model proposed can be used in smoothed particle simulations which are applicable on length and time scales significantly larger than those accessible in NEMD simulations. However, a tensorial generalization of the above model equation is needed. A theoretical foundation along the lines presented in Muschik (Ed.) (1993) is desirable.

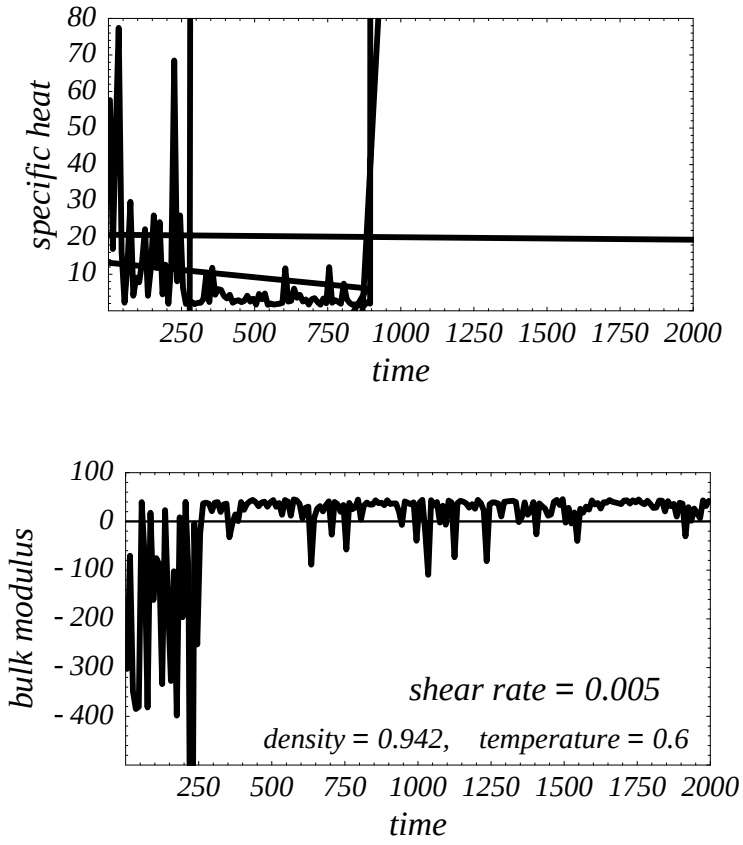

Figure 3: The specific heat and the bulk modulus as function of the time for the shear rate $\dot{\gamma} = 0.005$. All physical quantities are in standard LJ–units.

Acknowledgment

This work has been conducted under the auspices of the collaborative research projects Sfb 448 'Mesoskopisch strukturierte Verbundsysteme' and Sfb 605 'Elementarreibereignisse', financially supported by the Deutsche Forschungsgemeinschaft (DFG). This research was supported in part by the National Science Foundation under grant No. PHY99-07949.

Literature

1. Ackerson, B.J.; Loose, W.: Model calculations for the analysis of scattering data from layered structures, J. Chem. Phys., **101**, (1994), 7211.
2. Allen, M.P.; Tildesley, D.J.: Computer Simulation of Liquids, Clarendon, Oxford, (1987).
3. Ashurst, W.T.; Hoover, W.G.: Am. Phys. Soc., **17**, (1972), 1196; Argon Shear Viscosity via a Lennard-Jones Potential with Equilibrium and Nonequilibrium Molecular Dynamics, Phys. Rev. Lett., **31**, (1972), 206.
4. Ashurst, W.T.; Hoover, W.G.: Dense-fluid shear viscosity via nonequilibrium molecular dynamics, Phys. Rev. A, **11**, (1975), 658.
5. Binder, K.; Ciccotti G. (eds.): Monte Carlo and Molecular Dynamics of Condensed Matter Systems, IPS Conf. Proc. **49**, Bologna, (1996), pp. 825 - 841.
6. Born, M.: Statistical mechanics of liquids in their nonequilibrium state. Part I, J. Chem. Phys., **7**, (1939), 591.
7. Born, M.: Statistical mechanics of liquids in their nonequilibrium state. Part II, Proc. Camb. Phil. Soc., **36**, (1940), 160.

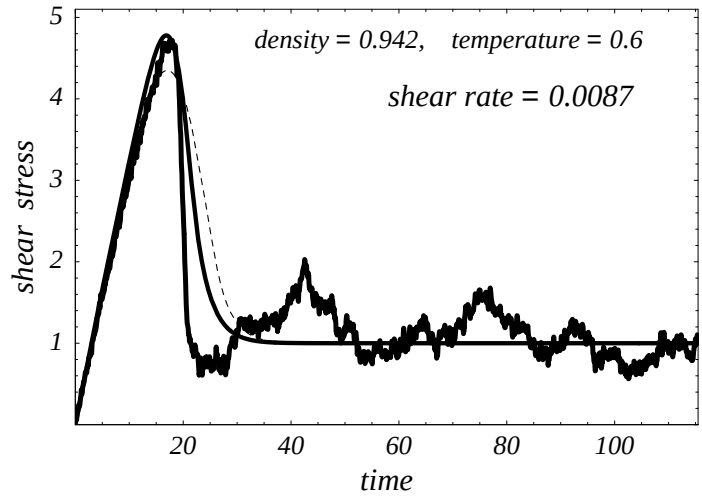

Figure 4: The shear stress as function of the time, computed in the NEMD simulation for $\dot{\gamma} = 0.0087$ compared with curves calculated by a model explained in the text. All physical quantities are in standard LJ–units.

8. Evans, D.J.; Morris, G.P.: Statistical Mechanics of Nonequilibrium Liquids, Academic Press, London, (1990).

9. Gosling, E.M.; McDonald, I.R.; Singer, K.: Calculation by molecular-dynamics of shear viscosity of a simple fluid, Mol. Phys., **26**, (1973), 1475.

10. Green, H.S.: The Molecular Theory of Fluids, North Holland, Amsterdam, (1952).

11. Green, M.S.: Markoff random processes and the statistical mechanics of time-dependent phenomena. II. Irreversible processes in fluids, J. Chem. Phys., **22**, (1954), 398.

12. Haberlandt, R.; Fritzsche, S.; Peinel, G.; Heinzinger, K: Molekular-Dynamik, Vieweg, Braunschweig, (1995).

13. Hess, O.; Loose, W.; Weider, T.; Hess S.: Shear-induced anisotropy of the structure of dense fluids, Physica B, **156/157**, (1989), 505.

14. Hess, S.; Loose, W.: Slip flow and slip boundary coefficient of a dense fluid via nonequilibrium molecular dynamics, Physica A, **162**, (1989), 138.

15. Hess, S.; Loose, W.: Flow properties and shear-induced structural changes in fluids: A case study on the interplay between theory, simulation, experiment, and applicatio, Ber. Bunsenges., Phys. Chem., **94**, (1990), 216.

16. Hess, S.: Constraints in Molecular Dynamics, Nonequilibrium Processes in Fluids via Computer Simulations, in: Computational Physics, eds. K.H. Hoffmann and M. Schreiber, Springer, Berlin, (1996) p. 268–293.

17. Hess, S.; Kröger, M.; Loose, W.; Pereira Borgmeyer, C.; Schramek, R.; Voigt, H.; Weider, T.: Simple and Complex Fluids under Shear, in K. Binder and G. Ciccotti (eds.) Monte Carlo and Molecular Dynamics of Condensed Matter Systems, IPS Conf. Proc., **49**, Bologna, (1996).

18. Hess, S.; Kröger, M.: Hoover, W.G.: Shear modulus of fluids and solids, Physica A, **239**, (1997), 449.

19. Hess. S.; Kröger, M.: Pressure of fluids and solids composed of particles interacting with a short range repulsive potential, Phys. Rev. E, **61**, (2000), 4629.

20. Hess, S.; Aust, C.; Bennett, L.; Kröger, M.; Pereira C., Borgmeyer, J.; Weider, T.: Rheology: From simple and to complex fluids, Physica A, **240**, (1997), 126.

21. Hess, S.: Flow properties and structure of anisotropic fluids studied by Non-Equilibrium Molecular Dynamics, and flow properties of other complex fluids: polymeric liquids, ferro-fluids and magneto-rheological fluids , in: P. Pasini and C. Zannoni (eds.) Advances in the computer simulations of liquid crystals, Nato Science Series, Series C: Mathematical and Physical Sciences, vol. **545**, Kluwer, Dordrecht, (2000), p. 189 - 233.

22. Hess. S; Kröger, M.: Thermophysical properties of gases, liquids, and solids composed of particles interacting with a short-range attractive potential, Phys. Rev., **64**, (2001), 011201.

23. Hoover, W.G.; Holt, A.C.; Squire, D.R.: Adiabatic elastic constants for argon. Theory and Monte Carlo calculations, Physica, **44**, (1969), 437.

24. Hoover, W.G.; Ashurst, W.T.: Dense fluid shear viscosity and thermal-conductivity - excess Theor. Chem. Adv. and Perspectives, **1**, (1975), 331.

25. Hoover, W.G.: Molecular Dynamics, Springer, Berlin, (1986).

26. Hoover, W.G.: Computational Statistical Mechanics, Elsevier, Amsterdam, (1991).

27. Hoover, W.G.: Nonequilibrium molecular dynamics - the 1st 25 years Physica A, **194**, (1993), 450.

28. Hoover, W.G.; Hess S.: Anisotropic plasticity with embedded-atom potentials, Physica A, **267**, (1999), 98.

29. J.E. Lennard–Jones: On an approximate intermolecular potential for Argon, Physica, **4**, (1937), 941.

30. Kröger, M.; Hess S.: Solid friction studied via non-equilibrium molecular dynamics computer simulations, ZAMM, **80**, Suppl. 1, (2000), 49-52.

31. Lees, A.W.; Edwards, S.F.: Transport Processes Under Extreme Conditions, J. Phys. C, **5**, (1972), 1921.

32. Loose, W.; Hess, S.: Velocity distribution function of a streaming gas via nonequilibrium molecular dynamics, Phys. Rev. Lett., **58**, (1988) 2443; Nonequilibrium velocity distribution function of gases: Kinetic theory and molecular dynamics, Phys. Rev. A, **37**, (1988), 2099.

33. Loose, W.; Hess, S.: Rheology of dense model fluids via nonequilibrium molecular dynamics: Shear thinning and ordering transition, Rheol. Acta, **28**, (1989), 91.

34. Loose, W.; Hess, S. in: Microscopic Simulation of Complex Flows, ed. M. Mareschal, ASI series, Plenum Press (1990).

35. Muschik, W. (Ed.): CISM courses and lectures **336**, Non-equilibrium thermodynamics with applications to solids, Springer, Berlin, (1993).

36. Schoen, M.; Hess S.; Diestler, D.J.: Rheological properties of confined thin films, Phys. Rev., **52**, (1995), 2587.

37. Squire, D.R.; Holt A.C.; Hoover, W.G.: Isothermal elastic constants for argon. Theory and Monte Carlo calculations. Physica, **42**, (1969), 388.

38. Stankovic, I.; Kröger, M.; Hess S.: Recognition and analysis of local structure in polycrystalline configurations, Comput. Phys. Commun., (2002), in press.

39. Zwanzig, R.; Mountain, R.D.: High-frequency elastic moduli of simple fluids, J. Chem. Phys., **43**, (1965), 4464.

Address: Prof. Dr. Siegfried Hess[1,3] and Dr. Martin Kröger, PD[1,2],
[1] Institut für Theoretische Physik, Fakultät Mathematik und Naturwissenschaften, Technische Universität Berlin, Hardenbergstr. 36, D-10623 Berlin, Germany;
[2] Polymer Physics, Material Sciences, ML H18, ETH Zürich, CH-8092 Zürich, Switzerland;
[3] S.Hess@physik.tu-berlin.de